Quasistellar spectrum for neutron activation measurements at $kT = 5$ keV

M. Heil,* S. Dababneh,† A. Juseviciute, F. Käppeler, and R. Plag
Forschungszentrum Karlsruhe, Institut für Kernphysik, Postfach 3640, D-76021 Karlsruhe, Germany

R. Reifarth
Los Alamos National Laboratory, Los Alamos, New Mexico 87545

S. O'Brien
University of Notre Dame, Physics Department, Notre Dame, Indiana, 46556

(Received 27 July 2004; revised manuscript received 29 November 2004; published 16 February 2005)

We have measured the neutron energy spectrum of the $^{18}O(p,n)^{18}F$ reaction at a proton energy of 2582 keV, 8 keV above the reaction threshold. At this energy the resulting neutron spectrum resembles almost perfectly a Maxwellian distribution at a thermal energy of $kT = 5.1 \pm 0.1$ keV. Since all neutrons are emitted in a forward cone of 140° opening angle, this reaction can be used for neutron activation measurements similar to the $^{7}Li(p,n)^{7}Be$ reaction, which is known for producing a thermal spectrum with $kT = 25$ keV. Measured neutron capture cross sections at $kT = 5.1$ keV and $kT = 25$ keV can be used to interpolate to $kT = 8$ keV, which characterizes the dominant neutron exposure during *s*-process nucleosynthesis in thermally pulsing low-mass AGB stars. In a first application of this new method the Maxwellian-averaged neutron capture cross section of ^{138}Ba was measured to be $\langle \sigma v \rangle / v_T = 13.0 \pm 0.5$ mb at $kT = 5.1$ keV.

DOI: 10.1103/PhysRevC.71.025803 PACS number(s): 29.25.Dz, 25.40.Lw, 26.20.+f

I. INTRODUCTION

Activation measurements with the $^{7}Li(p,n)^{7}Be$ reaction [1] as a neutron source have been successfully used to determine Maxwellian-averaged neutron capture cross sections (MACSs) corresponding to a thermal energy of $kT = 25$ keV. The superior sensitivity of this method compared to time-of-flight (TOF) experiments allowed measurements with extremely small cross sections or with samples as small as a few nanograms [2].

By assuming constant temperature and neutron flux as well as an exponential distribution of neutron exposures, the classical model of the *s* process provides a best fit of the observed abundance distribution with $kT = 29$ keV, or $T_8 = 3.3$ (in units of 10^8 K) [3]. For this case, experimental values obtained at $kT = 25$ keV could easily be extrapolated to the desired value of $kT = 29$ keV. The more complex stellar model of the main *s*-process component suggests that the neutrons are alternatively provided by the $^{13}C(\alpha,n)^{16}O$ and $^{22}Ne(\alpha,n)^{25}Mg$ reactions, which are activated at thermal energies of $kT = 8$ and 25 keV, respectively [4]. An extrapolation of the measured $kT = 25$ keV values down to $kT = 8$ keV is in principle possible, but it requires assumptions on the energy dependence of the capture cross section, which introduce significant additional uncertainties, in particular if the MACS is dominated by a few resonances [5].

Therefore, activation measurements of MACSs should preferably be performed as close to the thermal energy of $kT = 8$ keV as possible. This would also solve the persisting problem of the unknown energy dependence of partial neutron capture cross sections to isomeric states. Apart from a few exceptions [6], TOF experiments yield only the total neutron capture cross section. Partial cross-section measurements at $kT = 25$ keV are important for the analysis of a number of branchings in the *s*-process reaction chain. The corresponding isomeric ratios were found to exhibit large differences between thermal energies and the keV region [7,8]. Activation measurements are also important with respect to the direct capture (DC) channel, which is difficult to access by TOF studies but can account for a substantial portion of the total capture cross section for light nuclei or near magic neutron numbers.

This article describes the use of the $^{18}O(p,n)^{18}F$ reaction for activation measurements at lower stellar energies and illustrates its first application to the $^{138}Ba(n,\gamma)^{139}Ba$ cross section. The experimental setup for determining the neutron energy distribution of the $^{18}O(p,n)^{18}F$ reaction is outlined in Sec. II, and the verification of the Maxwellian energy distribution of $kT = 5.1$ keV is described in Sec. III. In Sec. IV the measurement of the ^{138}Ba cross section is presented. Section V gives a summary.

II. EXPERIMENTAL SETUP

The neutron energy distribution of the $^{18}O(p,n)^{18}F$ reaction was determined by a TOF experiment using the setup sketched in Fig. 1. The pulsed proton beam was provided by the Karlsruhe 3.7-MV Van de Graaff accelerator operated at an energy of 2582 keV with a repetition rate of 500 kHz, 1-ns pulse width, and an average beam current of 6 μA. The beam energy was calibrated via the threshold of the $^{18}O(p,n)^{18}F$ reaction at 2574 keV.

*Electronic address: Michael.Heil@ik.fzk.de.
†On leave from Faculty of Science and Information Technology, Al-Balqa Applied University, Salt 19117, Jordan.

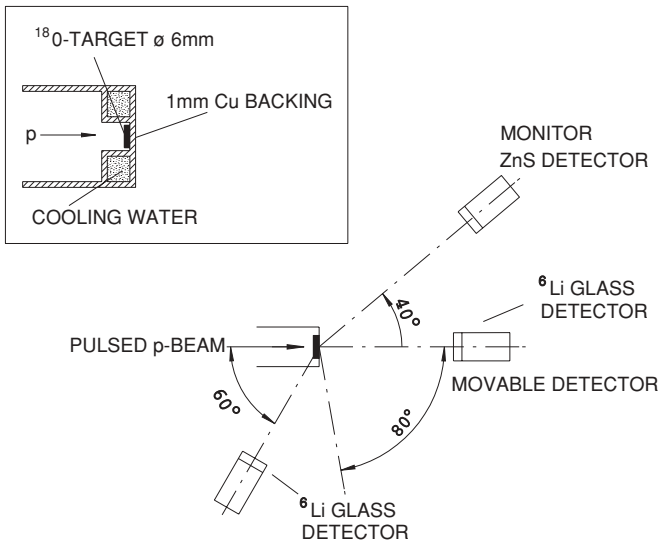

FIG. 1. Experimental setup to measure the neutron spectrum of the ^{18}O(p,n)^{18}F reaction. The inset in the top left corner shows details of the target construction.

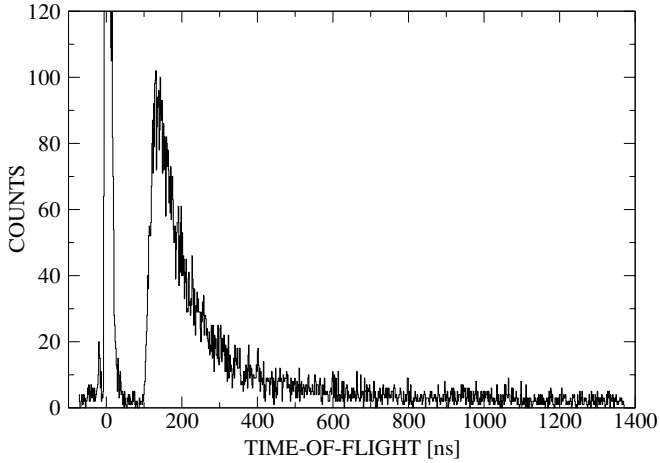

FIG. 2. Neutron TOF spectrum of the ^{18}O(p,n)^{18}F reaction taken at 30° with respect to the proton beam. The γ flash at time 0 and the onset of the neutron spectrum after 100 ns are clearly visible. The overall time resolution is 2 ns.

The target consisted of a 0.2-mm-thick tantalum disk with an oxide layer about 2 μm in thickness, which was produced by electrolysis of water with 95% enrichment in ^{18}O. The tantalum disk was glued onto a 1-mm-thick water-cooled copper backing as indicated in the inset of Fig. 1. The glue was suited for vacuum applications and was particularly selected to obtain good heat contact with the copper backing. The ring geometry of the cooling water ensured that neutron moderation was avoided since all neutrons are emitted in the forward direction. The forward emission results from the fact that the proton energy was chosen so close to the reaction threshold that the center-of-mass velocity of the neutrons was slower than the motion of the center-of-mass system.

In total three detectors were employed in this measurement. The neutron spectrum was determined by means of a movable ^{6}Li glass detector that was used to measure the angular distribution from 0° to 80° in steps of 10°. Located at a distance of 222 mm from the target, this detector covered an angle of 9.8° with respect to the ^{18}O target. Figure 2 shows the TOF spectrum obtained at 30° that was taken with an overall time resolution of 2 ns. A stationary neutron monitor detector was positioned 300 mm from the target at an angle of 40°. This ^{6}Li/ZnS detector was almost insensitive to γ rays and served for normalizing the individual spectra taken with the movable detector. A stationary ^{6}Li glass detector was mounted behind the neutron target at an angle of 120°, also at a distance of 222 mm. Located outside of the neutron cone, this detector was used for measuring the γ-ray background. Apart from the prompt γ flash, no time-correlated structures were found in the relevant part of the TOF spectra of this detector, thus confirming that a constant-γ background could be adopted in the final analysis.

III. NEUTRON SPECTRUM

The TOF measurements at different angles were first corrected for the neutron efficiency of the ^{6}Li glass detector by assuming a $1/v$ behavior of the efficiency in the considered energy range below 40 keV. After further corrections for solid angle and normalization to the flux measured by the monitor detector, the spectra were joined in the angle-integrated neutron spectrum, shown by the histogram in Fig. 3. The dashed line in Fig. 3 indicates a Maxwellian fit of the form

$$\Phi = cE_n e^{-E_n/kT}, \tag{1}$$

where E_n, kT, and c denote the neutron energy, the thermal energy, and a normalization constant, respectively. The best fit of the measured spectrum was obtained for a thermal energy of $kT = 5.1 \pm 0.1$ keV.

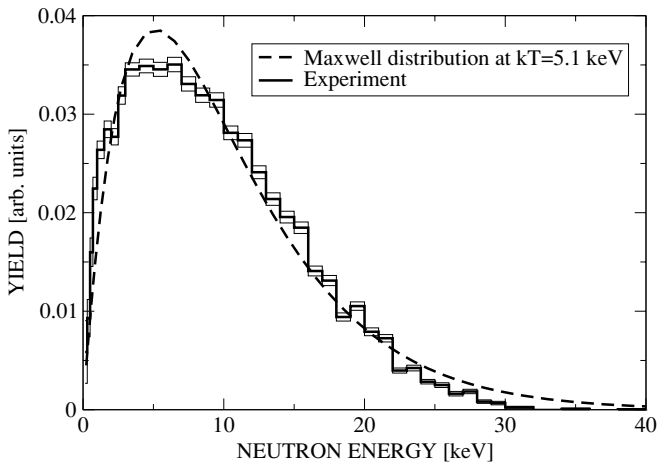

FIG. 3. Neutron energy spectrum of the ^{18}O(p,n)^{18}F reaction after integration of the entire neutron field up to the maximal emission angle (histogram). The dashed line represents the best fit of a Maxwellian spectrum with a thermal energy of $kT = 5.1$ keV.

TABLE I. Comparison of MACSs obtained with the experimental neutron spectrum and with an ideal Maxwell spectrum at $kT = 5.1$ keV.

c_1	c_2	Deviation (%)
1.0	0.0	2.35
0.9	0.1	0.32
0.8	0.2	0.55
0.7	0.3	1.04
0.6	0.4	1.35
0.5	0.5	1.56
0.4	0.6	1.72
0.3	0.7	1.84
0.2	0.8	1.93
0.1	0.9	2.01
0.0	1.0	2.07

In astrophysics, the relevant quantity, which enters into the stellar *s*-process models, is the MACS defined as

$$\frac{\langle \sigma v \rangle}{v_T} = \frac{2}{\sqrt{\pi}} \frac{\int_0^\infty \sigma(E_n) E_n \exp(-E_n/kT) dE_n}{\int_0^\infty E_n \exp(-E_n/kT) dE_n}, \quad (2)$$

where $\sigma(E_n)$ is the differential capture cross section, E_n is the total kinetic energy in the center-of-mass system, and $v_T = \sqrt{2kT/m}$ is the mean thermal velocity with the reduced mass m. The quality of the neutron spectrum obtained can be illustrated by comparing the astrophysically relevant MACSs for different cross-section shapes. For this purpose the MACSs were calculated for cross sections of the form

$$\sigma = c_1 \frac{1}{\sqrt{E_n}} + c_2 \sqrt{E_n}, \quad (3)$$

where c_1 and c_2 are multipliers of the s- and p-wave components, respectively. The calculated MACSs are then compared with the results obtained using a true Maxwell-Boltzmann distribution at $kT = 5.1$ keV (Table I).

The difference between the MACSs obtained with the experimental spectrum and with an ideal Maxwellian spectrum is at most 2.4%. This difference can be further reduced in practical applications, since all activations will be carried out relative to gold as a standard by the concomitant activation of gold foils attached to the sample.

IV. ACTIVATION MEASUREMENT

As a first application we present the measurement of the MACS of ^{138}Ba at a thermal energy of $kT = 5.1$ keV. The ^{138}Ba sample was chosen for several reasons. As a neutron magic isotope the neutron capture cross section of ^{138}Ba may well deviate from the $1/v$ law, which would imply large uncertainties in extrapolating the measured MACS from $kT = 25$ keV [1] to the required value at $kT = 8$ keV. This possibility can be checked by comparison with the MACS obtained in a recent TOF measurement [9]. In addition, the activation will provide a check for the assumption of a 10% direct capture contribution used in Ref. [9].

TABLE II. Sample dimensions.

Sample[a]	Mass (mg)	Uncertainty (%)
Ba_1	1474.4	0.1
Ba_2	1520.1	0.1
Au foils	typically 160	0.1

[a]All samples were 20 mm in diameter.

A. Samples and irradiations

Two samples were prepared from barium carbonate powder in the form of pressed pellets 20 mm in diameter and 1.5 mm in thickness. Immediately after pressing, the samples were enclosed in 0.1-mm-thick aluminum cans to prevent material losses during activation. The $BaCO_3$ was 98.04% enriched in ^{138}Ba. For the determination of the absolute neutron flux the samples were sandwiched between two 0.06-mm-thick gold foils of the same diameter (Table II).

The neutron field for the activation measurements was produced with the method described in Sec. II. The samples were placed 4.7 mm in front of the neutron production target to ensure that they were completely inside the neutron cone. Throughout the irradiations the neutron flux was monitored in steps of 5 s by means of a ^{6}Li glass detector at 1 m distance from the target. This information is required for evaluating the off-line corrections f_b [see Eq. (6)] for the decay of activated nuclei during the irradiations. The relevant parameters of the four activations are summarized in Table III.

B. Induced activity and data analysis

The induced activities in the barium sample and in the gold foils were measured using a system of two Clover-type HPGe detectors placed face-to-face in close geometry (Fig. 4). Each of the two detectors consists of four independent *n*-type Ge crystals in a common cryostat. The distance between the detector windows was defined by a 5.2-mm-thick sample holder, which was designed for the exact and reproducible positioning of the sample in the midplane of the system. The whole assembly was shielded against room background with 10 cm of lead. Figure 5 shows the γ-ray spectrum emitted by the activated barium sample from Run IV.

The net counts C_γ registered in the Clover detectors for a given characteristic γ-ray line can be expressed as

$$C_\gamma = A K_\gamma \epsilon_\gamma I_\gamma (1 - e^{-\lambda t_M}) e^{-\lambda t_w}, \quad (4)$$

TABLE III. Relevant parameters of the neutron irradiations.

Activation	Ba sample	Duration (min)	Integrated flux (in units of 10^9)	
			Front Au foil	Rear Au foil
Run I	Ba_1	172	0.533	0.395
Run II	Ba_1	181	1.265	0.920
Run III	Ba_2	212	0.388	0.294
Run IV	Ba_2	196	1.413	1.018

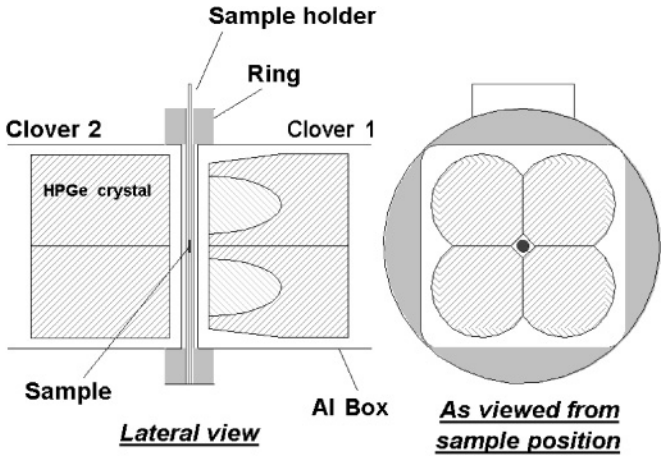

FIG. 4. Schematic setup for measuring the induced barium and gold activities with two HPGe Clover detectors in close geometry with the sample positioned in the midplane.

where A is the total number of activated nuclei, K_γ is the correction factor for self-absorption, ϵ_γ is the peak efficiency of the Clover detector system, and I_γ is the γ-ray intensity per decay. The waiting time between the irradiation and the measurement is denoted by t_W, and the actual measuring time is denoted by t_M. The decay parameters used in data analysis are listed in Table IV. For the 165-keV transition in the decay of ^{139}Ba the intensity was adopted from Ref. [10], although a significantly larger uncertainty is quoted in the compilation of Ref. [11].

The total number of activated nuclei is given by

$$A = \Phi_{\rm tot} N \sigma f_b, \tag{5}$$

where $\Phi_{\rm tot} = \int \Phi(\mathrm{t}) dt$ is the time-integrated neutron flux, N is the number of sample atoms per square centimeter, and σ is the spectrum-averaged neutron capture cross section. The factor

$$f_b = \frac{\int_0^{t_B} \Phi(t) e^{-\lambda(t_B - t)} dt}{\int_0^{t_B} \Phi(t) dt} \tag{6}$$

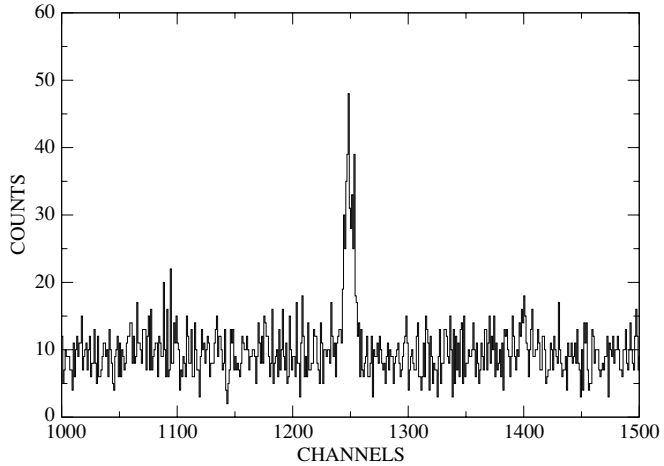

FIG. 5. The γ spectrum of the activated barium sample from run II showing the 165.86-keV line from the decay of ^{139}Ba.

TABLE IV. Decay properties of the product nuclei.

Product nucleus	Half-life	γ-ray energy (keV)	I_γ per decay (%)
^{138}Ba	83.06 ± 0.28 min	165.86	23.76 ± 0.25[a]
^{197}Au	2.69517 ± 0.00021 d	411.80	95.58 ± 0.12[b]

[a]Ref. [10].
[b]Ref. [12].

corrects for the decay of activated nuclei during the irradiation time t_B, including the effect of variations in the neutron flux. The correction f_b was calculated from the neutron yield measured with the ^{6}Li glass detector at a 1-m distance from the target in intervals of 60 s throughout the irradiation. The integrated neutron flux is determined by the activation of the gold foils on both sides of the sample. The peak efficiency ϵ_γ was measured with a set of standard calibration sources. For the 165.86-keV line in the decay of ^{139}Ba (Table IV) and for the 412-keV line in the decay of ^{198}Au the absolute efficiency was $(46.0 \pm 0.7)\%$ and $(19.6 \pm 0.3)\%$, respectively.

The effect of γ-ray self-absorption K_γ and of the extended geometry of the barium and gold samples has been evaluated by means of Monte Carlo simulations using the GEANT4 toolkit [13]. For this purpose the detection setup was carefully modeled, including the rather complex Clover geometry [14] as well as the dimensions and the exact positioning of the sample relative to the Ge crystals. The corresponding corrections were obtained by generating γ rays at the center of the sample holder with the proper decay energies. A total of 10^7 primary events were generated at the position of the calibration point source and the energy deposited in the individual Ge crystals was histogrammed. Then, the $BaCO_3$ sample with its thin Al capsule and the gold samples were simulated accordingly by assuming a homogeneous activation of the samples. The correction factor for each sample was obtained by comparing the intensity of the γ line in the spectrum of the point source with that of the spectra of the actual samples. Correction factors of 0.895 and 0.994 were found for the barium and the gold samples, respectively. The larger correction for the barium sample is expected because of the larger sample thickness and the lower γ-ray energy.

Summing effects in the Ge detectors are negligible since the decays of ^{139}Ba and ^{198}Au are completely dominated by single γ transitions.

C. Results and discussion

With a 50-μA proton beam current a neutron flux of 10^5 s^{-1} cm^{-2} was obtained with the ^{18}O$(p,n)^{18}$F reaction, a factor of about 10^4 lower than the flux produced with the ^{7}Li$(p,n)^7$Be reaction [8]. This drawback can partly be compensated by measuring the induced activities with high-efficiency detection systems (Fig. 4).

The cross section values from different activations are summarized in Table V.

The gold cross section is well known for neutron energies above 2.7 keV [15,16] and is, therefore, used as a standard

TABLE V. Activations and results.

Activation	Sample	Cross section (mb)	Uncertainty	
			stat. (%)	syst. (%)
Run I	Ba_1	11.4	6.4	5.0
Run II	Ba_1	12.8	4.6	4.4
Run III	Ba_2	14.8	8.1	4.7
Run IV	Ba_2	12.9	3.0	4.4
Average		13.0	3.0	3.9

for activation measurements with the ^{7}Li(p,n)^{7}Be neutron source. To evaluate the average for activations at $kT = 5.1$ keV the energy-dependent capture cross section of ^{197}Au is also needed for lower energies down to 0.1 keV. Since no reliable experimental data are presently available in this energy region, the evaluated cross section of the ENDF/B database was used in the full energy region but was normalized to reproduce the measured MACS of 582 ± 9 mb at $kT = 30$ keV [16]. With the normalization factor of 0.954 the resulting MACS of ^{197}Au at $kT = 5.1$ keV is

$$\frac{\langle \sigma v \rangle}{v_T} = 2028 \pm 50\,\text{mb}.$$

We note, however, that an accurate measurement at lower neutron energies is underway to establish the gold cross section as a standard also for activation measurements at $kT =$ 5.1 keV [17].

The overall uncertainty of the final cross section is dominated by the counting statistics and the systematic uncertainty of the neutron flux at the sample position. For thin samples the latter is usually estimated to be 25% of the difference between the flux values measured with the two gold foils. Because of the 1.5-mm-thick Ba sample, this approach would have resulted in a systematic uncertainty of 8%. To better quantify this uncertainty, a stack of gold foils, which were separated by 0.5 mm, was activated separately. The deduced neutron yields versus distance from the target is plotted in Fig. 6. Based on

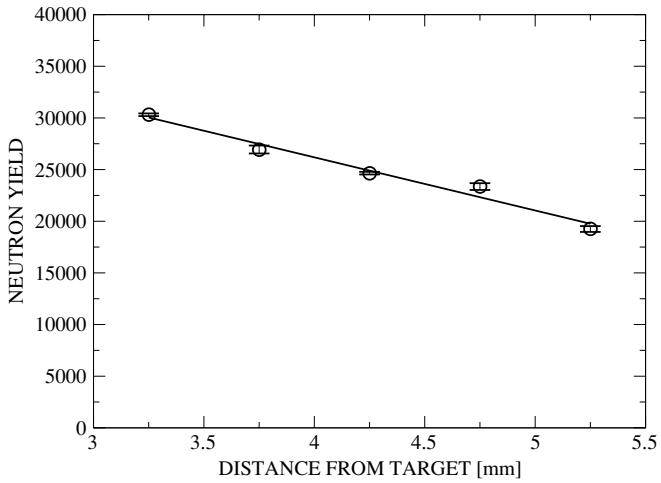

FIG. 6. The neutron yield measured with a stack of equally spaced gold foils. The line shows a linear fit to the data points.

TABLE VI. Compilation of uncertainties.

Source of uncertainty	Uncertainty (%)	
	Au	^{138}Ba
Counting statistics[a]	0.5	3.0
Gold cross section	2.5	
Number of sample atoms	<0.1	<0.1
γ-ray intensity per decay	0.1	1.0
Time factors f_w, f_m, f_b	<0.1	<0.1
Summing effects	<0.1	<0.1
Detector efficiency	1.5	1.5
Divergence of neutron flux[a]		1.4
Total uncertainty		3.8

[a]After combining the data of Runs I–IV.

this information the systematic uncertainty for the divergence of the flux could be reduced to the average uncertainty of the neutron flux measurements with the two gold samples. The various uncertainties are listed in Table VI.

The MACS of ^{138}Ba was obtained as the average of the activations performed in Runs I–IV. The final value at $kT =$ 5.1 keV,

$$\frac{\langle \sigma v \rangle}{v_T}(^{138}\text{Ba}) = 13.0 \pm 0.5\,\text{mb},$$

exhibits an uncertainty of 3.8% and is in fair agreement with the value of 13.6 ± 0.5 mb measured via the TOF method [9]. However, only the resonant part is considered by the uncertainty of the TOF value, whereas an additional 3% may be estimated for the 10% contribution from the DC component. Fully including the DC component is in the result of the activation measurement suggests that the DC part was overestimated in Ref. [9].

V. SUMMARY

For a proton energy of 2582 keV, the ^{18}O(p,n)^{18}F reaction was demonstrated to closely simulate a Maxwellian neutron energy distribution with a thermal energy of $kT =$ 5.1 ± 0.1 keV. This provides an additional important neutron source for measuring stellar (n,γ) rates in the region of thermal energies characteristic of s-process nucleosynthesis in thermally pulsing low-mass AGB stars, complementing the well-known ^{7}Li(p,n)^{7}Be reaction, which yields a Maxwell distribution for $kT = 25$ keV. As a first application, the MACS of ^{138}Ba at $kT = 5.1$ keV was measured to be 13.0 ± 0.5 mb. This value is in fair agreement with the 13.6 ± 0.5 mb obtained in a TOF measurement, which, however, neglected the sizable uncertainty from the estimated DC contribution. The DC contribution is quantitatively taken into account in the present result.

ACKNOWLEDGMENTS

We thank H.-P. Knaetsch, D. Roller, and W. Seith for their support during the activations at the Van de Graaff accelerator,

as well as R. Gallino for many discussions concerning the astrophysics issues. This work was supported by the Joint Institute for Nuclear Astrophysics (JINA) through NSF Grants No. PHY-0072711 and PHY-0228206. The hospitality of Forschungszentrum Karlsruhe is gratefully acknowledged by S.O. and S.D.

[1] H. Beer and F. Käppeler, Phys. Rev. C **21**, 534 (1980).
[2] R. Reifarth *et al*., Astrophys. J. **582**, 1251 (2003).
[3] C. Arlandini *et al*., Astrophys. J. **525**, 886 (1999).
[4] R. Gallino *et al*., Astrophys. J. **497**, 388 (1998).
[5] P. E. Koehler *et al*., Nucl. Phys. **A621**, 258 (1997).
[6] K. Wisshak *et al*., Phys. Rev. C **61**, 065801 (2000).
[7] H. Beer, Astrophys. J. **375**, 823 (1991).
[8] R. Reifarth and F. Käppeler, Phys. Rev. C **66**, 054605 (2002).
[9] H. Beer, F. Corvi, and P. Mutti, Astrophys. J. **474**, 843 (1997).
[10] R. Gehrke, Int. J. Appl. Radiat. Isotopes **31**, 37 (1980).
[11] T. Burrows, Nucl. Data Sheets **92**, 623 (2001).
[12] Z. Chunmei, Nucl. Data Sheets **95**, 59 (2002).
[13] Technical report, CERN, GEANT home page: http://wwwinfo.cern.ch/asd/geant4/geant4.html.
[14] S. Dababneh *et al*., Nucl. Instrum. Methods A **517**, 230 (2004).
[15] R. L. Macklin, private communication to S. F. Mughabghab (unpublished).
[16] W. Ratynski and F. Käppeler, Phys. Rev. C **37**, 595 (1988).
[17] U. Abbondanno *et al*., Phys. Rev. C (in preparation).